Control of Deep-Hysteresis Aeroengine Compressors[1]

Hsin-Hsiung Wang[2]
Department of Electronic Engineering,
Oriental Inst. of Technology,
58, Sec. 2, Szu-Chuan Road,
Panchiao, Taipei County, 220 Taiwan
e-mail: swang@www.ee.oit.edu.tw

Miroslav Krstić
Department of AMES,
University of California, San Diego,
La Jolla, CA 92093-0411
e-mail: krstic@ucsd.edu

Michael Larsen
Department of ECE,
University of California,
Santa Barbara, CA 93106
e-mail: larsenm@seidel.ece.ucsb.edu

Frequencies of higher-order modes of fluid dynamic phenomena participating in aeroengine compressor instabilities far exceed the bandwidth of available (affordable) actuators. For this reason, most of the heretofore experimentally validated control designs for aeroengine compressors have been via low-order models—specifically, via the famous Moore-Greitzer cubic model (MG3). While MG3 provides a good qualitative description of open-loop dynamic behavior, it does not capture the main difficulties for control design. In particular, it fails to exhibit the so-called ''right-skew'' property which distinguishes the deep hysteresis observed on high-performance axial compressors from a small hysteresis present in the MG3 model. In this paper we study fundamental feedback control problems associated with deep-hysteresis compressors. We first derive a parametrization of the MG3 model which exhibits the right skew property. Our approach is based on representing the compressor characteristic as a convex combination of a usual cubic polynomial and a nonpolynomial term carefully chosen so that an entire family of right-skew compressors can be spanned using a single parameter ϵ. Then we develop a family of controllers which are applicable not only to the particular parametrization, but to general Moore-Greitzer type models with arbitrary compressor characteristics. For each of our controllers we show that it achieves a supercritical (soft) bifurcation, that is, instead of an abrupt drop into rotating stall, it guarantees a gentle descent with a small stall amplitude. Two of the controllers have novel, simple, sensing requirements: one employs only the measurement of pressure rise and rotating stall amplitude, while the other uses only pressure rise and the mass flow rate (1D sensing). Some of the controllers which show excellent results for the MG3 model fail on the deep-hysteresis compressor model, thus justifying our focus on deep-hysteresis compressors. Our results also confirm experimentally observed difficulties for control of compressors that have a high value of Greitzer's B parameter. We address another key issue for control of rotating stall and surge—the limited actuator bandwidth—which is critical because even the fastest control valves are often too slow compared to the rates of compressor instabilities. Our conditions show an interesting trade-off: as the actuator bandwidth decreases, the sensing requirements become more demanding. Finally, we go on to disprove a general conjecture in the compressor control community that the feedback of mass flow rate, known to be beneficial for shallow-hysteresis compressors, is also beneficial for deep-hysteresis compressors. [S0022-0434(00)03101-4]

1 Introduction

In recent years, aeroengine compressor systems have become a subject of major interest to control engineers. There are two types of instability in compressors—*rotating stall* and *surge*. While surge can lead to compressor damage, rotating stall can cause a sudden drop in performance. Feedback control can be helpful in avoiding the two instability phenomena over a wide operating envelope.

A basic understanding of the effects of rotating stall can be gained by considering the operating characteristic in Fig. 2. Since the optimal operation objective (at given speed) is to increase the pressure rise Ψ, the operating point is moved along the axisymmetric characteristic to lower values of flow Φ. If the operating point is moved beyond the peak,[3] the compressor drops into a regime with drastically reduced pressure rise. Moreover, an attempt to immediately return to the regime of high pressure is defeated by the presence of a hysteresis.

Frequencies of higher-order modes of fluid dynamic phenomena participating in rotating stall and surge far exceed the bandwidth of available actuators. At the same time, as observed experimentally, low order modes are encountered first. For this reason, a meaningful (or at least tractable) approach to control design is via low-order models. The simplest model that adequately describes the basic dynamics of rotating stall and surge and their interaction is the three-state nonlinear model of Moore and Greitzer [1]—MG3—which is a Galerkin approximation of a higher-order PDE model. Even though this model represents a simplification of the dynamics of a real compressor, it has been the cornerstone of some of the most successful feedback control designs which have been validated experimentally. Liaw and Abed [2] developed a local bifurcation-based controller that changes the character of the bifurcation at the stall inception point, from hard subcritical to soft supercritical, thus avoiding an abrupt transition into rotating stall. Badmus et al. [3] experimentally validated this design on a low-speed compressor and Eveker et al.developed an improved version of this design which prevents surge on high-speed compressors. A controller of Krstić et al. [5] achieves global stability and has more modest sensing requirements but is restricted to cubic compressor characteristics proposed by Moore and Greitzer [1].

Many experimental compressors (Mansoux et al. [6], Behnken et al. [7]) have non-cubic characteristics that create a deeper hysteresis in the rotating stall diagram. Figure 2 gives an example of an experimental characteristic (Behnken et al. [7]) for a compres-

[1]This work was supported in part by AFOSR, NSF, and ONR.

[2]This work was performed while this author was a doctoral student at University of Maryland.

[3]Which would be a violation of the stall margin.

Contributed by the Dynamic Systems and Control Division for publication in the JOURNAL OF DYNAMIC SYSTEMS, MEASUREMENT, AND CONTROL. Manuscript received by the Dynamic Systems and Control Division July 15, 1996. Associate Technical Editor: R. S. Chandran.

sor in the laboratory of Richard Murray at California Institute of Technology. The deep hysteresis denoted by diamonds is not seen on a corresponding MG3 model.

It was first observed by Jankovic [8] that the deeper hysteresis introduces a fundamental obstacle to control design. The source of this obstacle is a (nonlinear) nonminimum-phase property not present in the MG3 model. Sepulchre and Kokotović [9] developed a ''two-sine'' model that can describe deep-hysteresis compressors in the region of nominal operation and explored conditions for feedback stabilization of these compressors. However, the model in Sepulchre and Kokotović [9], involves hard-to-handle Bessel functions, and does not maintain continuity with the basic MG3 model for which a wealth of knowledge on bifurcations and nonlinear dynamics already exists (McCaughan [10]).

In this paper, we first develop a new parametrization of the MG3 model (we refer to it as ϵ-MG3) which is based on a convex combination of the cubic compressor characteristic and another simple but nonpolynomial function. With this combination, we can achieve compressor characteristics which can be used to model compressors with the deep-hysteresis property. Like Sepulchre and Kokotovic [9], our model uses a single parameter ϵ to describe an entire family of compressors.

Then we develop a family of controllers which are applicable not only to the particular ϵ-MG3 parametrization, but also to general Moore-Greitzer type one-mode models with arbitrary compressor characteristics. For each of our controllers we show that it achieves a supercritical (soft) bifurcation, that is, instead of an abrupt drop into rotating stall, it guarantees a gentle descent with a small stall amplitude.

Our designs require minimal modeling knowledge—only the angles of arrival of the stall characteristic at the stall inception point—which are easy to determine from experimental bifurcation diagrams. Our objective is to relax the sensing requirements of the controller of Eveker et al. [4], and we accomplish this objective in two ways: one of our designs does not require the measurement of the mass flow rate $\dot{\Phi}$, while the other does not require the measurement of the rotating stall amplitude R. Our results confirm experimentally observed difficulties for control of compressors that have a high value of Greitzer's B parameter.

We also address another key issue for control of rotating stall and surge—the limited actuator bandwidth—which is critical because even the fastest control valves are often too slow compared to the rates of compressor instabilities. Our conditions show an interesting trade-off: as the actuator bandwidth decreases, the sensing requirements become more demanding.

Finally, we address a general conjecture in the compressor control community (based on the dramatic results of Eveker et al. [4]) that, since feedback of $\dot{\Phi}$ is beneficial for a shallow-hysteresis compressor, it may be also beneficial for a deep-hysteresis compressor. We investigate this conjecture by studying the stability interval under the stall inception point on the stall branch, and show that the conjecture is not true.

2 A General Moore-Greitzer Three-State Model

The simplest model that adequately describes the dynamics of rotating stall and surge in axial-flow compression systems shown in Fig. 1 is the three-state Moore-Greitzer [1] model:

$$\dot{R} = \sigma R \mathcal{F}(R,\Phi) \tag{1}$$

$$\dot{\Phi} = -\Psi + \mathcal{G}(R,\Phi) \tag{2}$$

$$\dot{\Psi} = \frac{1}{\beta^2}(\Phi - \Phi_T), \tag{3}$$

where the functions $\mathcal{F}(R,\Phi)$ and $\mathcal{G}(R,\Phi)$ are given by

$$\mathcal{F}(R,\Phi) = \frac{1}{3\pi\sqrt{R}} \int_0^{2\pi} \Psi_C(\Phi + 2\sqrt{R}\sin\theta)\sin\theta\, d\theta \tag{4}$$

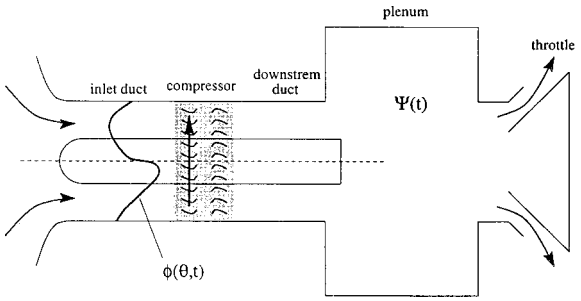

Fig. 1 Compression system

Table 1 Notation in the Moore-Greitzer model

$\Phi = \hat{\Phi}/W - 1 - \Phi_{C0}$	$\hat{\Phi}$—annulus-averaged flow coefficient W—compressor characteristic semi-width
$\Psi = \hat{\Psi}/H$	$\hat{\Psi}$—plenum pressure rise H—compressor characteristic semi-height
$A = \hat{A}/W$	$\hat{A}$—rotating stall amplitude
Φ_T	mass flow through the throttle/$W-1$
θ	angular (circumferential) position
$\beta = \frac{2H}{W}B$	B—Greitzer stability parameter
$\sigma = \frac{3l_c}{m+\mu}$	l_c—effective length of inlet duct normalized by compressor radius m—Moore expansion parameter μ—compressor inertia within blade passage
$t = \frac{H}{Wl_c}\hat{t}$	$\hat{t}$—(actual time)×(rotor angular velocity)

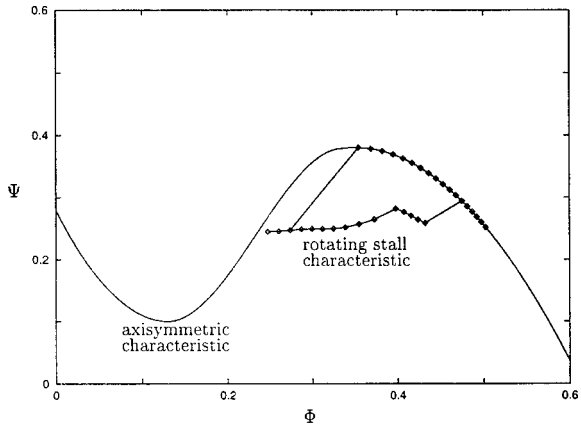

Fig. 2 Axisymmetric and rotating stall characteristics of an experimental compressor at Caltech. The stall characteristic exhibits deep hysteresis.

$$\mathcal{G}(R,\Phi) = \frac{1}{2\pi} \int_0^{2\pi} \Psi_C(\Phi + 2\sqrt{R}\sin\theta)\, d\theta. \tag{5}$$

The quantities appearing in this model are listed in Table 1, with $R = (A/2)^2$.

Equation (3) is mass conservation in the plenum: the time rate of change in plenum pressure is proportional to the difference between mass flow entering and exiting the plenum. Equation (2) is a momentum balance: the acceleration of the fluid in the up-

stream and downstream ducts is proportional to the difference in the pressure rise across the compressor and the pressure rise in the plenum. The steady-state, annulus-averaged pressure rise across the compressor is given via the *S*-shaped compressor characteristic $\Phi_C(\cdot)$ shown as the solid curve in Fig. 2. Equation (1) is obtained from the same momentum balance PDE as (2) by applying the Galerkin approximation.

The throttle flow Φ_T is related to the pressure rise Φ through the throttle characteristic

$$\Psi = \frac{1}{\gamma^2}(1+\Phi_{C0}+\Phi_T)^2, \tag{6}$$

where γ is the throttle opening. We will be applying control action by varying the opening γ.

3 The ϵ-MG3 Model Parametrization

In this section we introduce a special parametrization of the MG3 model that allows an elegant characterization of deep-hysteresis compressors and will be used for simulation tests. Note that our future control design will not be restricted to this parametrization but will be applicable to general MG3 models.

A standard compressor characteristic introduced by Moore and Greitzer is the cubic characteristic

$$\Psi_C(\Phi) = \Psi_{C0} + 1 + \frac{3}{2}\Phi - \frac{1}{2}\Phi^3. \tag{7}$$

This characteristic is adequate only for shallow-hysteresis compressors. We replace it by a convex combination of a cubic characteristic (7) and the function $2\Phi/(1+\Phi^2)$:

$$\Psi_C(\Psi) = \Psi_{C0} + 1 + (1-\epsilon)\left(\frac{3}{2}\Phi - \frac{1}{2}\Phi^3\right) + \epsilon\frac{2\Phi}{1+\Phi^2} \tag{8}$$

where $\epsilon \in [0,1]$. The function $2\Phi/(1+\Phi^2)$ is carefully chosen so that:

1 the integrals in (1) and (2) have a closed-form solution,
2 it exhibits the qualitative properties of deep-hysteresis compressors,
3 it retains a connection with the familiar cubic characteristic. In particular, both $\frac{3}{2}\Phi - \frac{1}{2}\Phi^3$ and $2\Phi/(1+\Phi^2)$ achieve extrema ± 1 at $\Phi = \pm 1$.

After extensive calculations, employing MATHEMATICA to solve integrals in closed form,[4] the compressor model becomes

$$\begin{aligned}\dot{R} = \sigma\Bigg\{ & (1-\epsilon)R(1-\Phi^2-R) \\ & + \frac{2\epsilon}{3}\Bigg[1 - \frac{1}{\sqrt{2}[(\Phi^2-4R-1)^2+4\Phi^2]^{1/2}} \\ & \times((((\Phi^2-1)(\Phi^2-4R-1)+4\Phi^2)^2+64\Phi^2R^2)^{1/2} \\ & + (\Phi^2-1)(\Phi^2-4R-1)+4\Phi^2)^{1/2}\Bigg]\Bigg\}\end{aligned} \tag{9}$$

$$\begin{aligned}\dot{\Phi} = & -\Psi + \Psi_{C0} + 1 + (1-\epsilon)\left(\frac{3}{2}\Phi - \frac{1}{2}\Phi^3 - 3\Phi R\right) \\ & + \epsilon\frac{\sqrt{2}\,\mathrm{sgn}(\Phi)}{[(\Phi^2-4R-1)^2+4\Phi^2]^{1/2}}\{[(\Phi^2-4R-1)^2+4\Phi^2]^{1/2} \\ & + (\Phi^2-4R-1)\}^{1/2}\end{aligned} \tag{10}$$

[4]The details are omitted here because of the journal page constraints; see Wang et al. [11] for an outline of the main steps.

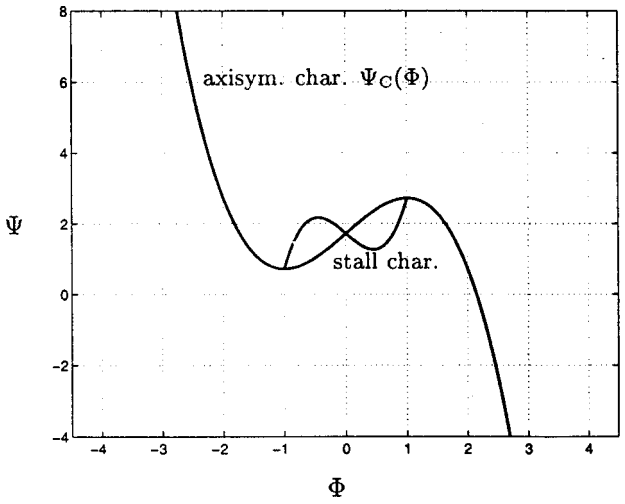

Fig. 3 Equilibria of the ϵ-MG3 model with $\epsilon = 0$

$$\dot{\Psi} = \frac{1}{\beta^2}(\Phi - \Phi_T). \tag{11}$$

We refer to this model as the ϵ-MG3 model. Note that, even though (10) contains sgn(Φ), this equation is not discontinuous because the term multiplied by sgn(Φ) vanishes at $\Phi = 0$ for all values of *R*. For $\epsilon = 0$, the model (9)–(11) reduces to the standard MG3 model

$$\dot{R} = \sigma R(1-\Phi^2-R) \tag{12}$$

$$\dot{\Phi} = -\Psi + \Psi_{C0} + 1 + \frac{3}{2}\Phi - \frac{1}{2}\Phi^3 - 3\Phi R \tag{13}$$

$$\dot{\Psi} = \frac{1}{\beta^2}(\Phi - \Phi_T). \tag{14}$$

There are two sets of equilibria of the model (9)–(11). The no-stall equilibria are

$$\begin{bmatrix} R \\ \Phi \\ \Psi \end{bmatrix}_e = \begin{bmatrix} 0 \\ \Phi_0 \\ \Psi_C(\Phi_0) \end{bmatrix}, \quad \Phi_0 \in \mathbb{R}. \tag{15}$$

The stall equilibria are

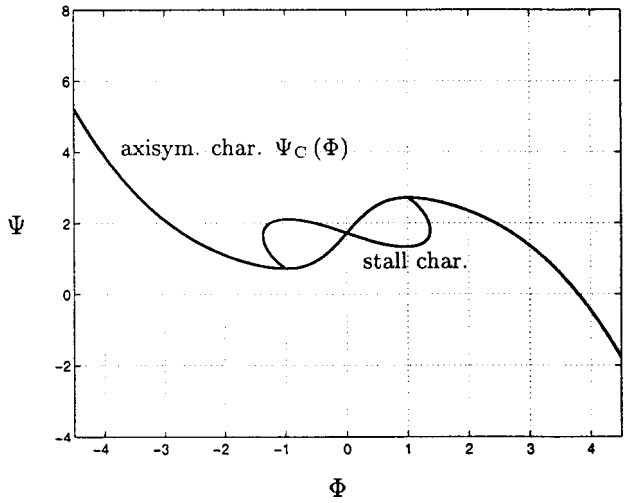

Fig. 4 Equilibria of the ϵ-MG3 model with $\epsilon = 0.9$

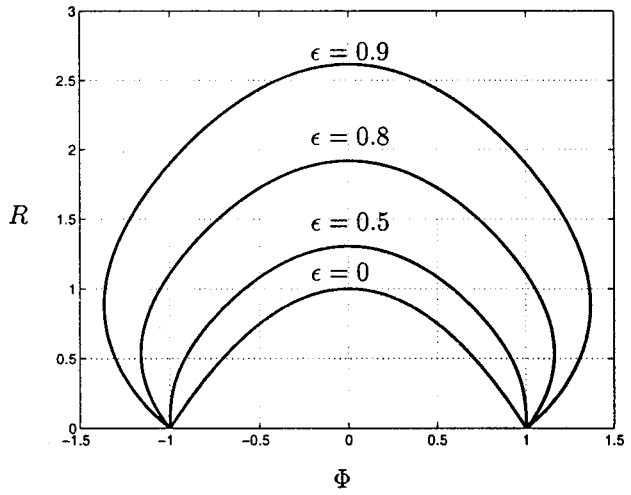

Fig. 5 R vs Φ relationship with varying ϵ

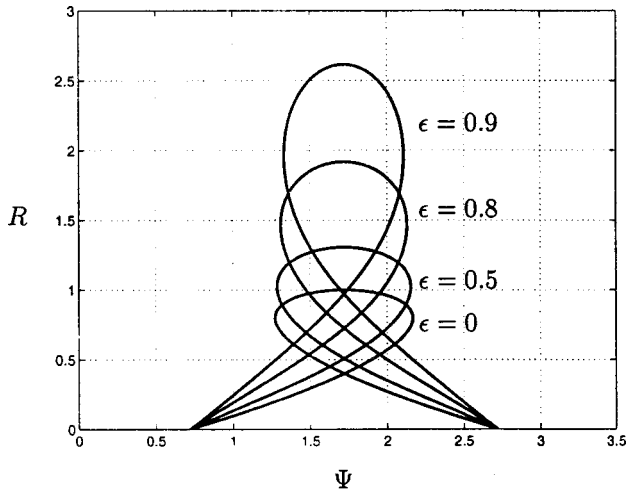

Fig. 6 R vs Ψ relationship with varying ϵ

$$\begin{bmatrix} R \\ \Phi \\ \Psi \end{bmatrix}_e = \begin{bmatrix} R_0 \\ \Phi_{R\pm}(R_0) \\ \Psi_{R\pm}(R_0) \end{bmatrix}, \quad R_0 \in [0, \vec{R}]. \tag{16}$$

The functions $\Phi_{R+}(R)$ and $\Phi_{R-}(R)$ are obtained as solutions of (9) with $\dot{R}=\sigma R\mathcal{F}(R,\Phi)=0$ and $R\neq 0$. Note that since $\mathcal{F}(R,\Phi)$ in (9) is a function of Φ^2, we get two solutions $\Phi_{R-}(R) = -\Phi_{R+}(R)$. The functions $\Psi_{R+}(R)$ and $\Psi_{R-}(R)$ are obtained as solutions of (10) with $\dot{\Phi}=-\Psi+\mathcal{G}(R,\Phi)=0$, that is, by substituting $\Phi=\Phi_{R\pm}(R)$ into $\Psi=\mathcal{G}(R,\Phi)$. The plots of equilibria of the ϵ-MG3 model are given in Fig. 3 ($\epsilon=0$) and Fig. 4 ($\epsilon=0.9$). The corresponding $R(\Phi)$ curves and $R(\Phi)$ curves are shown in Fig. 5 and Fig. 6, respectively.

4 Critical Slopes and ''Skewness''

A critical parameter for the control of a compressor model is the ''direction'' of the stall characteristic at the stall inception point. We now determine the slope of the projection of the stall characteristic to each of the three coordinate planes:

$$S_1=\left.\frac{d\Phi_{R+}(R)}{dR}\right|_{R=0} \tag{17}$$

Table 2 Critical slopes as functions of ϵ

		$\epsilon=0$	$\epsilon=1$
S_1	$-1.5\dfrac{\epsilon-0.5}{\epsilon-1.5}$	-0.5	1.5
S_2	$2(\epsilon-1.5)$	-3	-1
S_3	$-\dfrac{4}{3}\dfrac{(\epsilon-1.5)^2}{(\epsilon-0.5)}$	6	-0.67

$$S_2=\left.\frac{d\Psi_{R+}(R)}{dR}\right|_{R=0} \tag{18}$$

$$S_3=\left.\frac{d\Psi_S(\Phi)}{d\Phi}\right|_{\Phi=1}=\frac{S_2}{S_1}, \tag{19}$$

where $\Psi_S(\Phi)$ is the stall characteristic shown in Figs. 3 and 4. After lengthy calculations, for the ϵ-MG3 parametrization we obtain the critical slopes as functions of ϵ_1 listed in Table 2.

A key property affecting the ability to design feedback controllers for compressor models is the slope S_1, which we refer to as ''skewness'' of the compressor characteristics. A compressor with $S_1<0$ is said to be ''left-skew,'' while a compressor with $S_1>0$ is referred to as ''right-skew.''

For a general compressor characteristic (not necessarily ϵ-MG3), the critical slopes would be defined as

$$S_1=-\left.\frac{\dfrac{\partial\mathcal{F}(R,\Phi)}{\partial R}}{\dfrac{\partial\mathcal{F}(R,\Phi)}{\partial\Phi}}\right|_{\substack{R=0\\ \Phi=1}} \tag{20}$$

$$S_2=\left.\frac{\partial\mathcal{G}(R,\Phi)}{\partial R}\right|_{\substack{R=0\\ \Phi=1}}. \tag{21}$$

Routine calculations show that in case of ϵ-MG3 one obtains the expressions in Table 2.

5 Open-Loop Bifurcation Diagrams for Throttle Opening γ as Parameter

We consider a three-stage compressor studied in Meyers et al. [12] whose parameters are $\Psi_{C0}=0.72$ and $\sigma=4$. We study both a

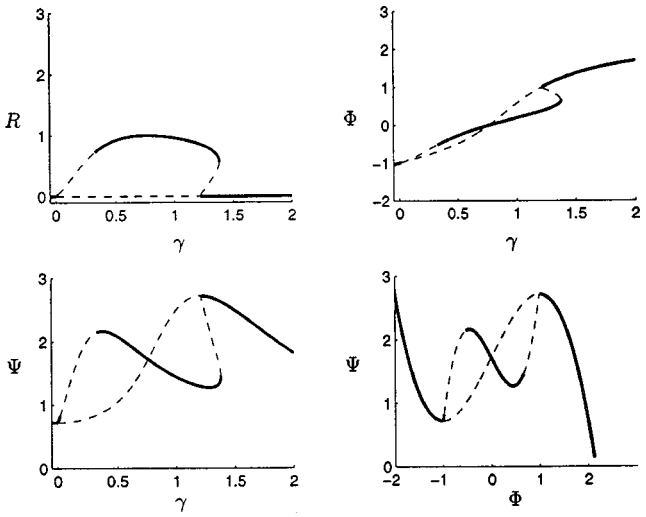

Fig. 7 Bifurcation diagrams for the open-loop system with $\epsilon=0$ and $\beta=0.71$. The throttle opening γ is the bifurcation parameter.

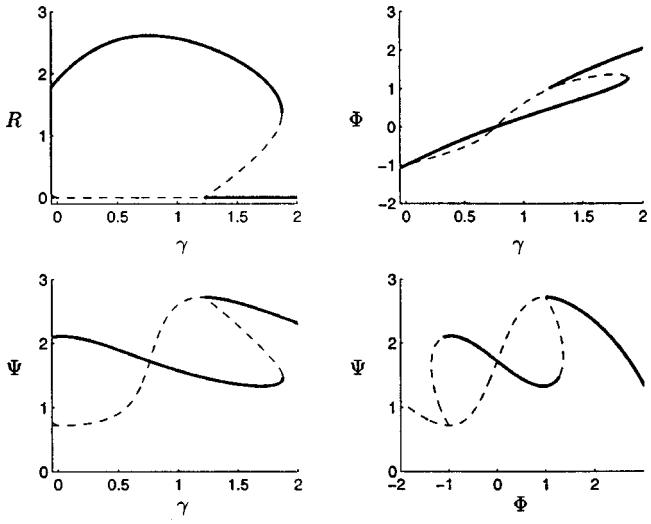

Fig. 8 Bifurcation diagrams for the open-loop system with $\epsilon = 0.9$ and $\beta = 0.71$

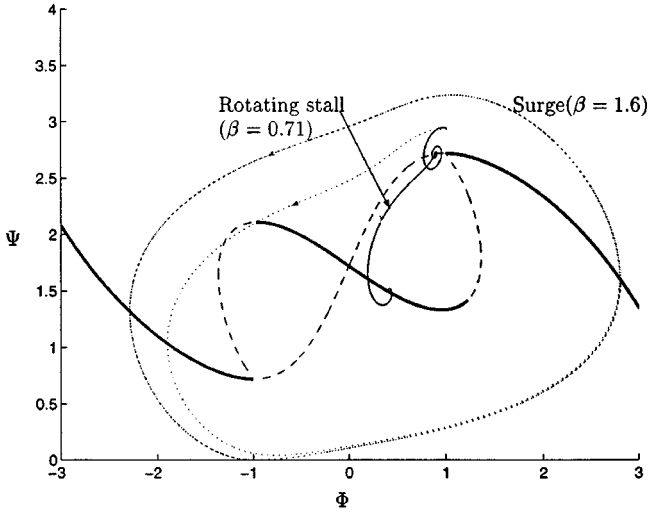

Fig. 9 Transient responses for throttle opening $\gamma = 1.15$, slightly below the value for the stall inception point. A low value of β ($\beta = 0.71$) results in rotating stall, while a high value of β ($\beta = 1.6$) results in surge.

low-speed case $\beta = 0.71$ and a high-speed case $\beta = 1.42$, and both a left-skew case $\epsilon = 0$ and a right-skew case $\epsilon = 0.9$. Figure 7 shows the diagrams for $\epsilon = 0$, $\beta = 0.71$. The solid thick line represents stable equilibria, while the dashed thin line represents unstable equilibria. Figure 8 is for the right-skew case $\epsilon = 0.9$ with the same low $\beta = 0.71$. The right-skew case results in a much deeper hysteresis; while for $\epsilon = 0$ the interval of γ participating in the hysteresis is 0.17, for $\epsilon = 0.9$ it is 0.66, which indicates that a recovery from rotating stall for $\epsilon = 0.9$ would be much more difficult. For a right-skew ($\epsilon = 0.9$) high-speed ($\beta = 1.42$) case, there is only a slight difference in the bifurcation diagram (not shown) relative to Fig. 8.

However, the transient behavior for the low-speed ($\beta = 0.71$) and high-speed ($\beta = 1.6$) cases is quite different, with the former resulting in rotating stall while the latter results in surge, as shown in Fig. 9. Note that the trajectory for $\beta = 0.71$ is strongly influenced by the presence of a saddle point on the axisymmetric characteristic, just left from the peak.

6 Control Design

A full-state feedback controller for the model (1)–(3) would employ the measurements of all three states, R, Φ, and Ψ, for feedback. In addition, the experiments in (Eveker et al. [4]) show that $\dot{\Phi}$ can be measured successfully and used for feedback.

However, we are motivated to look for partial-state feedback controllers to reduce the sensing requirements. For example, for left-skew compressors, we showed in Krstic et al. [5] that stabilization is possible using a controller of the form

$$\gamma = \frac{\Gamma + \overline{\beta}^2 (c_\Psi \Psi - c_\Phi \Phi)}{\sqrt{\Psi}}, \tag{22}$$

i.e., without using R and $\dot{\Phi}$. As we shall see in this paper, controlling a right-skew compressor will require a measurement of either R or $\dot{\Phi}$. Thus, we postulate that the controller will be of the form

$$\gamma = \frac{\Gamma + \overline{\beta}^2 (c_\Psi \Psi - c_\Phi \Phi + c_R R - d_\Phi \dot{\Phi})}{\sqrt{\Psi}}. \tag{23}$$

The controller development in this section is independent of the form of compressor characteristic. We only require that $\Psi_C'(1) = 0$ and $\Psi_C''(1) < 0$, i.e., that $\Psi_C(\Phi)$ has a maximum at $\Phi = 1$.

6.1 Enforcing a Supercritical Bifurcation. With the controller (23), the system (1)–(3) becomes

$$\dot{R} = \sigma R \mathcal{F}(R, \Phi) \tag{24}$$

$$\dot{\Phi} = -\Psi + \mathcal{G}(R, \Phi) \tag{25}$$

$$\dot{\Psi} = \frac{\overline{\beta}^2}{\beta^2} \left(-c_R R + c_* \Phi - c_\Psi \Psi + d_\Phi \dot{\Phi} \right) + \frac{1 + \Phi_{C0} - \Gamma}{\beta^2}, \tag{26}$$

where

$$c_* = c_\Phi + \frac{1}{\overline{\beta}^2}. \tag{27}$$

Let us consider an equilibrium on the stall characteristic. The equilibrium is determined by the value of Γ, which is given as

$$\Gamma(R_0) = 1 + \Phi_{C0} + \overline{\beta}^2 [-c_R R_0 + c_* \Phi_{R+}(R_0) - c_\psi \Psi_{R+}(R_0)] \tag{28}$$

at an equilibrium with $R = R_0$. In order for the bifurcation at the stall inception point to have a supercritical character with respect to Γ, we need to achieve

$$\lim_{R \to 0^+} \frac{d\Gamma(R)}{dR} < 0. \tag{29}$$

Noting that

$$\lim_{R \to 0^+} \frac{d\Gamma(R)}{dR} = -\overline{\beta}^2 (c_R - S_1 c_* + S_2 c_\psi), \tag{30}$$

we conclude that the bifurcation will be supercritical if and only if

$$c_R - S_1 c_* + S_2 c_\Psi > 0. \tag{31}$$

Since large Γ means lower stall amplitude R, we also require that in no-stall operation Φ increases with Γ (accompanied by a decreasing pressure rise Ψ). In other words, we consider an axisymmetric equilibrium with

$$\Gamma(\Phi_0) = 1 + \Phi_{C0} + \overline{\beta}^2 (c_* \Phi_0 - c_\Psi \Psi_C(\Phi_0)) \tag{32}$$

and require that

$$\lim_{\Phi\to 1^+}\frac{d\Gamma(\Phi)}{d\Phi}>0. \tag{33}$$

Noting that

$$\lim_{\Phi\to 1^+}\frac{d\Gamma(\phi)}{d\Phi}=\overline{\beta}^2 c_*, \tag{34}$$

we conclude with the requirement

$$c_*>0. \tag{35}$$

6.2 Linearization at a Stall Equilibrium. We consider an equilibrium $R=R_0$, $\Phi=\Phi_{R+}(R_0)$, $\Psi=\Psi_{R+}(R_0)$ and define the error coordinates

$$r=R-R_0 \tag{36}$$

$$\Phi=\Phi-\Phi_{R+}(R_0) \tag{37}$$

$$\psi=\Psi-\Psi_{R+}(R_0). \tag{38}$$

The linearization of the system (24)–(26) is readily shown to be

$$\dot{r}=-a_1(R_0)(-\Sigma_1(R_0)r+\phi) \tag{39}$$

$$\dot{\phi}=(\Sigma_2(R_0)+a_2(R_0)\Sigma_1(R_0))r-a_2(R_0)\phi-\psi \tag{40}$$

$$\dot{\psi}=\kappa(-c_R r+c_*\phi-c_\Psi\psi+d_\Phi\dot{\phi}), \tag{41}$$

where $\kappa=(\overline{\beta}/\beta)^2$ and

$$a_1(R)=-\sigma R\left.\frac{\partial\mathcal{F}(R,\Phi)}{\partial\Phi}\right|_{\Phi=\Phi_{R+}(R)} \tag{42}$$

$$a_2(R)=-\left.\frac{\partial\mathcal{G}(R,\Phi)}{\partial\Phi}\right|_{\Phi=\Phi_{R+}(R)} \tag{43}$$

$$\Sigma_1(R)=-\left.\frac{\dfrac{\partial\mathcal{F}(R,\Phi)}{\partial R}}{\dfrac{\partial F(R,\Phi)}{\partial\Phi}}\right|_{\Phi=\Phi_{R+}(R)}=\frac{d\Phi_{R+}(R)}{dR} \tag{44}$$

$$\Sigma_2(R)=\left.\frac{\partial\mathcal{G}(R,\Phi)}{\partial R}\right|_{\Phi=\Phi_{R+}(R)}+\left.\frac{\partial\mathcal{G}(R,\Phi)}{\partial F}\right|_{\Phi=\Phi_{R+}(R)}\frac{d\Phi_{R+}(R)}{dR}=\frac{d\Psi_{R+}(R)}{dR}. \tag{45}$$

Before we derive our stabilization criteria, we establish some fundamental properties of the functions $a_1(R)$, $a_2(R)$, $\Sigma_1(R)$, and $\Sigma_2(R)$. As everything else in this paper, these properties are independent of a specific form of the compressor characteristic.

Lemma 6.1. For a compressor characteristic that has a maximum at $\Phi=1$, that is, with $\Psi_C'(1)=0$ and $\Psi_C''(1)<0$, we have the following properties for the functions $a_1(R)$, $a_2(R)$, $\Sigma_1(R)$, and $\Sigma_2(R)$ at the stall inception point:

$$a_1(0)=0 \tag{46}$$

$$a_2(0)=0 \tag{47}$$

$$\Sigma_1(0)=S_1=-\frac{1}{2}\frac{\Psi_C'''(1)}{\Psi_C''(1)} \tag{48}$$

$$\Sigma_2(0)=S_2=\Psi_C''(1) \tag{49}$$

$$a_1'(0)=-\frac{2\sigma}{3}S_2>0 \tag{50}$$

$$a_2'(0)=S_1S_2 \tag{51}$$

$$\Sigma_1'(0)=\frac{5}{4}S_1^3-\frac{1}{4S_2}\left(3S_1\Psi_C^{(4)}(1)+\frac{5}{12}\Psi_C^{(5)}(1)\right) \tag{52}$$

$$\Sigma_2'(0)=-3S_1^2S_2+\frac{1}{2}\Psi_C^{(4)}(1) \tag{53}$$

Proof: We start by rewriting (4) and (5) as

$$\mathcal{F}(A^2/4,\Phi)=\frac{1}{3\pi}\frac{2}{A}\int_0^{2\pi}\Psi_C(\Phi+A\sin\theta)\sin\theta d\theta \tag{54}$$

$$\mathcal{G}(A^2/4,\Phi)=\frac{1}{2\pi}\int_0^{2\pi}\Psi_C(\Phi+A\sin\theta)d\theta. \tag{55}$$

Then, the partial derivatives necessary for (42)–(45) are

$$\frac{\partial\mathcal{F}(A^2/4,\Phi)}{\partial\Phi}=\frac{1}{3\pi}\frac{2}{A}\int_0^{2\pi}\Psi_C'(\Phi+A\sin\theta)\sin\theta d\theta \tag{56}$$

$$\frac{\partial\mathcal{F}(A^2/4,\Phi)}{\partial R}=\frac{2}{A}\frac{1}{3\pi}\left[\frac{2}{A}\int_0^{2\pi}\Psi_C'(\Phi+A\sin\theta)\sin^2\theta d\theta-\frac{2}{A^2}\int_0^{2\pi}\Psi_C(\Phi+A\sin\theta)\sin\theta d\theta\right] \tag{57}$$

$$\frac{\partial\mathcal{G}(A^2/4,\Phi)}{\partial\Phi}=\frac{1}{2\pi}\int_0^{2\pi}\Psi_C'(\Phi+A\sin\theta)d\theta \tag{58}$$

$$\frac{\partial\mathcal{G}(A^2/4,\Phi)}{\partial R}=\frac{1}{\pi A}\int_0^{2\pi}\Psi_C'(\Phi+A\sin\theta)\sin\theta d\theta. \tag{59}$$

When substituted into (42)–(45), all these expressions have to be evaluated at $\Phi=\Phi_{R+}(R)=\Phi_{R+}(A^2/4)$. The second term in (57) will become zero by definition of the function Φ_{R+}. Hence, we only need the function $\Psi_C'(\Phi_{R+}(A^2/4)+A\sin\theta)$. Since the Taylor expansion of Φ_{R+} is $\Phi_{R+}(A^2/4)=1+\Sigma_1(0)A^2/4+\frac{1}{2}\Sigma_1'(0)(A^2/4)^2+O(A^6)$, the function Ψ_C' can be approximated by

$$\begin{aligned}
&\Psi_C'\left(1+A\sin\theta+S_1\frac{A^2}{4}+\frac{1}{2}\Sigma_1'(0)\left(\frac{A^2}{4}\right)^2+O(A^6)\right)\\
&=\Psi_C''(1)\left[A\sin\theta+S_1\frac{A^2}{4}+\frac{1}{2}\Sigma_1'(0)\left(\frac{A^2}{4}\right)^2+O(A^6)\right]\\
&\quad+\frac{1}{2}\Psi_C'''(1)\left[A\sin\theta+S_1\frac{A^2}{4}+\frac{1}{2}\Sigma_1'(0)\left(\frac{A^2}{4}\right)^2+O(A^6)\right]^2\\
&\quad+\frac{1}{6}\Psi_C^{(4)}(1)\left[A\sin\theta+S_1\frac{A^2}{4}+\frac{1}{2}\Sigma_1'(0)\left(\frac{A^2}{4}\right)^2+O(A^6)\right]^3\\
&\quad+\frac{1}{24}\Psi_C^{(5)}(1)\left[A\sin\theta+S_1\frac{A^2}{4}+\frac{1}{2}\Sigma_1'(0)\left(\frac{A^2}{4}\right)^2+O(A^6)\right]^4\\
&\quad+O\left(\left[A\sin\theta+S_1\frac{A^2}{4}+\frac{1}{2}\Sigma_1'(0)\left(\frac{A^2}{4}\right)^2+O(A^6)\right]^5\right)\\
&=\Psi_C'(1)\sin\theta A+\left(\frac{1}{4}\Psi_C''(1)S_1+\frac{1}{2}\Psi_C'''(1)\sin^2\theta\right)A^2\\
&\quad+\left(\frac{1}{4}\Psi_C'''(1)S_1\sin\theta+\frac{1}{6}\Psi_C^{(4)}(1)\sin^3\theta\right)A^3\\
&\quad+\left(\frac{1}{32}\Psi_C''(1)\Sigma_1'(0)+\frac{1}{32}\Psi_C'''(1)S_1^2+\frac{1}{12}\Psi_C^{(4)}(1)S_1\sin^2\theta\right.\\
&\quad\left.+\frac{1}{24}\Psi_C^{(5)}(1)\sin^4\theta\right)A^4+O(A^5).
\end{aligned} \tag{60}$$

By substituting (60) into (56)–(59), we get

$$\left.\frac{\partial \mathcal{F}(R,\Phi)}{\partial \Phi}\right|_{\Phi=\Phi_{R+}(R)} = \frac{2}{3}\left[\Psi_C''(1)+\left(\Psi_C'''(1)S_1+\frac{1}{2}\Psi_C^{(4)}(1)\right)R\right] + O(R^2) \tag{61}$$

$$\left.\frac{\partial \mathcal{F}(R,\Phi)}{\partial \mathrm{P}}\right|_{\Phi=\Phi_{R+}(R)} = \frac{1}{3}\left[\Psi_C''(1)S_1+\frac{3}{2}\Psi_C'''(1)+\left(\frac{1}{2}\Psi_C''(1)\Sigma_1'(0) + \frac{1}{2}\Psi_C'''(1)S_1^2+\Psi_C^{(4)}(1)S_1 + \frac{5}{12}\Psi_C^{(5)}(1)\right)R\right]+O(R^2) \tag{62}$$

$$\left.\frac{\partial \mathcal{G}(R,\Phi)}{\partial \Phi}\right|_{\Phi=\Phi_{R+}(R)} = (\Psi_C''(1)S_1+\Psi_C'''(1))R+O(R^2) \tag{63}$$

$$\left.\frac{\partial \mathcal{G}(R,\Phi)}{\partial \mathrm{P}}\right|_{\Phi=\Phi_{R+}(R)} = \Psi_C''(1)+\left(\Psi_C'''(1)S_1+\frac{1}{2}\Psi_C^{(4)}(1)\right)R + O(R^2). \tag{64}$$

By substituting (61) into (42), we get

$$a_1(R) = -\frac{2\sigma}{3}\Psi_C''(1)R+O(R^2). \tag{65}$$

By substituting (63) into (43), we get

$$a_2(R) = -(\Psi_C''(1)S_1+\Psi_C'''(1))R+O(R)^2. \tag{66}$$

By substituting (61) and (62) into (44), we get

$$\Sigma_1(R) = -\left(\frac{1}{2}S_1+\frac{3}{4}\frac{\Psi_C'''(1)}{\Psi_C''(1)}\right)+\frac{1}{2\Psi_C''(1)}\left[\left(S_1+\frac{3}{2}\frac{\Psi_C'''(1)}{\Psi_C''(1)}\right)\times\left(\Psi_C'''(1)S_1+\frac{1}{2}\Psi_C^{(4)}(1)\right)-\left(\frac{1}{2}\Psi_C''(1)\Sigma_1'(0) + \frac{1}{2}\Psi_C'''(1)S_1^2+\Psi_C^{(4)}(1)S_1+\frac{5}{12}\Psi_C^{(5)}(1)\right)\right]R+O(R^2). \tag{67}$$

Since $\Sigma_1(0)=S_1=-(\frac{1}{2}S_1+\frac{3}{4}\Psi_C'''(1)/\Psi_C''(1))$, we get

$$S_1 = -\frac{1}{2}\frac{\Psi_C'''(1)}{\Psi_C''(1)}. \tag{68}$$

In a similar fashion, we determine $\Sigma_1'(0)$ and get

$$\Sigma_1(R) = -\frac{1}{2}\frac{\Psi_C'''(1)}{\Psi_C''(1)}+\left[\frac{5}{4}S_1^3-\frac{1}{4S_2}\left(3\Psi_C^{(4)}(1)S_1+\frac{5}{12}\Psi_C^{(5)}(1)\right)R\right]+O(R^2). \tag{69}$$

Finally, by substituting (64), (66), and (69) into (45), we get

$$\Sigma_2(R) = \Psi_C''(1)+\left(\frac{3}{2}\Psi_C'''(1)S_1+\frac{1}{2}\Psi_C^{(4)}(1)\right)R+O(R^2) \triangleq S_2+\left(-3S_1^2S_2+\frac{1}{2}\Psi_C^{(4)}(1)\right)R+O(R^2). \tag{70}$$

We conclude the proof by noting that (50) and (51) are obtained by substituting $S_1=-\frac{1}{2}\Psi_C'''(1)/\Psi_C''(1)$ and $S_2=\Psi_C''(1)$ into (65) and (66). ■

Now we turn our attention to the stability conditions for the linearized model (39)–(41). Substituting (40) into (41), we get the Jacobian of the system (24)–(26):

$$\begin{bmatrix} a_1\Sigma_1 & -a_1 & 0 \\ \Sigma_2+a_2\Sigma_1 & -a_2 & -1 \\ \kappa[(\Sigma_2+a_2\Sigma_1)d_\Phi-c_R] & \kappa(c_*-a_2d_\Phi) & -\kappa(d_\phi+c_\Psi) \end{bmatrix}. \tag{71}$$

The characteristic polynomial of the Jacobian (71) is

$$p(s) = s^3+[\kappa(d_\Phi+c_\Psi)+(a_2-a_1\Sigma_1)]s^2 + [\kappa c_*+\kappa(a_2-a_1\Sigma_1)c_\Psi+a_1(\Sigma_2-\kappa\Sigma_1 d_\Phi)]s + \kappa a_1(c_R-\Sigma_1 c_*+\Sigma_2 c_\Psi). \tag{72}$$

By applying the Routh-Hurwitz method, the necessary and sufficient conditions for stability of the system (39)–(41) are

$$\kappa(d_\Phi+c_\Psi)+(a_2-a_1\Sigma_1)>0 \tag{73}$$

$$\kappa c_*+\kappa(a_2-a_1\Sigma_1)c_\Psi+a_1(\Sigma_2-\kappa\Sigma_1 d_\Phi)>0 \tag{74}$$

$$\kappa a_1(c_R-\Sigma_1 c_*+\Sigma_2 c_\Psi)>0 \tag{75}$$

$$[\kappa(d_\Phi+c_\Psi)+(a_2-a_1\Sigma_1)][\kappa c_*+\kappa(a_2-a_1\Sigma_1)c_\Psi + a_1(\Sigma_2-\kappa\Sigma_1 d_\Phi)]-[\kappa a_1(c_R-\Sigma_1 c_*+\Sigma_2 c_\Psi)]>0 \tag{76}$$

Since, by Lemma 6.1,

$$a_2(R)-a_1(R)\Sigma_1(R) = O(R), \tag{77}$$

then

$$c_\Psi+d_\Phi>0 \tag{78}$$

guarantees that (73) is satisfied near the stall inception point. Noting that

$$a_1(R) = a_1'(0)R+O(R^2), \tag{79}$$

and that

$$\Sigma_1(R) = S_1+O(R) \tag{80}$$

$$\Sigma_2(R) = S_2+O(R), \tag{81}$$

we conclude that the condition

$$c_*>0 \tag{82}$$

guarantees that condition (74) is satisfied near the stall inception point. Furthermore, since $a_1'(0)>0$, the condition

$$c_R-S_1c_*+S_2c_\Psi>0 \tag{83}$$

guarantees that condition (75) is satisfied near the stall inception point. Noting that the expression in (76) is $\kappa^2(d_\Phi+c_\Psi)c_* + O(R)$, we conclude that it is satisfied near the stall inception point whenever (78) and (82) are satisfied. We point out that condition (83) coincides with the bifurcation condition (31), and (82) coincides with (35). The stability conditions are summarized in Table 3.

Table 3 The stability conditions for the system (24)–(26)

$c_R-S_1\left(c_\Phi+\frac{1}{\overline{\overline{\beta^2}}}\right)+S_2c_\Psi>0$
$c_\Phi+\frac{1}{\overline{\overline{\beta^2}}}>0$
$c_\Psi+d_\Phi>0$

6.3 Stability at the Bifurcation Point. Our analysis showed that we can stabilize stall equilibria near the stall inception point but it did not include the stall inception point itself because $a_1(0)=0$ implies that the characteristic polynomial (72) has one root at $s=0$. For the stall inception point, the analysis based on linearization is inconclusive. Therefore, at this point we apply a center manifold technique.

The one-dimensional center manifold of the equilibrium $R=0$, $\Phi=1$, and $\Psi=\Psi_C(1)$ of the system (24)–(26) is readily shown to belong to

$$\Phi(R)=1+\frac{c_R+S_2c_\Psi}{c_*}R+O(R^2) \tag{84}$$

$$\Psi(R)=\Psi_C(1)+S_2R+O(R^2). \tag{85}$$

Then its reduced system becomes

$$\dot{R}=\frac{2}{3}\sigma S_2\left[\frac{c_R-S_1c_*+S_2c_\Psi}{c_*}+O(R)\right]R^2. \tag{86}$$

Since $\Psi_C''(1)=S_2<0$, the system (86) is asymptotically stable if the stability conditions of Table 3 are satisfied. Therefore, by the reduction principle (Khalil [13], Theorem 4.2), the equilibrium $R=0$, $\Phi=1$, $\Psi=\Psi_C(1)$ of (24)–(26) is asymptotically stable.

7 A Family of Controllers

In Section 6 we showed that the control law (23) with gains satisfying the conditions in Table 3 enforces a supercritical bifurcation at the stall inception point and stabilizes an interval of stall equilibria near this point. Our main objective is to extract partial-state feedback controllers from the family given by (23). Our focus is on right-skew compressors for which $S_1>0$ and $S_2<0$.

7.1 The (Ψ,R)-Controller. The choice of gains

$$c_\Phi=d_\Phi=0,\quad c_R>0,\quad c_\Psi>0,$$

$$c_R-S_1\frac{1}{\overline{\beta^2}}+S_2c_\Psi>0,$$

satisfies the conditions in Table 3. Thus, the control law

$$\gamma=\frac{\Gamma+\overline{\beta^2}(c_\Psi\Psi+c_RR)}{\sqrt{\Psi}},\quad c_R+S_2c_\Psi>\frac{S_1}{\overline{\beta^2}} \tag{87}$$

is stabilizing.

7.2 The (Ψ,$\dot{\Phi}$)-Controller. The choice of gains

$$c_\Phi=c_R=0,\quad c_\Psi<0,\quad d_\Phi>0,$$

$$-S_1\frac{1}{\overline{\beta^2}}+S_2c_\Psi>0,\quad c_\Psi+d_\Phi>0$$

satisfies the conditions in Table 3. Thus, the control law

$$\gamma=\frac{\Gamma+\overline{\beta^2}(c_\Psi\Psi-d_\Phi\dot{\Phi})}{\sqrt{\Psi}} \tag{88}$$

is locally stabilizing. However, the linear dependence of the numerator on Ψ is undesirable because it creates undesirable additional equilibria. For this reason, we replace (88) by

$$\gamma=\frac{\Gamma+\mathcal{N}_\Psi(\Psi)-d_\Phi(\dot{\Phi})}{\sqrt{\Psi}} \tag{89}$$

where $\mathcal{N}_\Psi(\Psi)$ is a nonlinear function which needs to satisfy

$$\mathcal{N}_\Psi'(2+\Psi_{C0})<\frac{S_1}{S_2}=\frac{1}{S_3} \tag{90}$$

$$\mathcal{N}_\Psi'(2+\Psi_{C0})+\overline{\beta^2}d_\Phi>0. \tag{91}$$

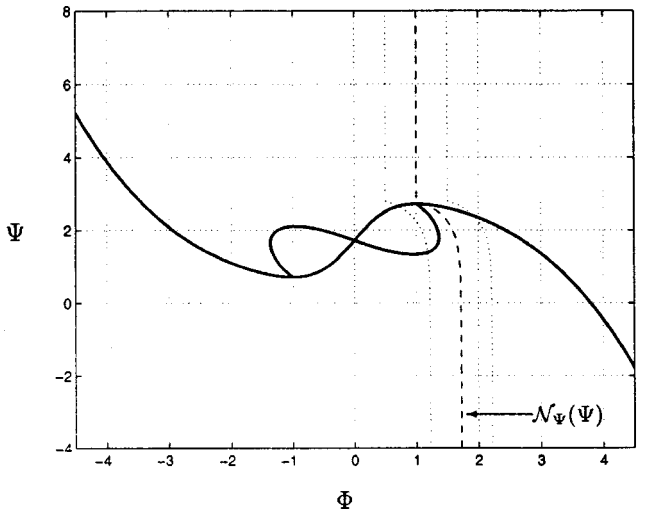

Fig. 10 The function $\mathcal{N}_\Psi(\Psi)$. Variations in Γ result in no more than one stall and one axisymmetric equilibrium.

A qualitative sketch of $\mathcal{N}_\Psi(\Psi)$ is given in Fig. 10. This function is chosen as monotonically nonincreasing. In presence of variations in Γ,$\mathcal{N}_\Psi(\Psi)$ will ensure that there is never more than one stall equilibrium and one axisymmetric equilibrium. If $\mathcal{N}_\Psi(\Psi)$ were linear in Ψ, this would allow a creation of a second axisymmetric equilibrium.

At this point it is not clear whether $\dot{\Phi}$ is harder to measure than Φ. With a Φ-term in the control law

$$\gamma=\frac{\Gamma+\mathcal{N}_\Psi(\Psi)-\overline{\beta^2}(c_\Phi\Phi+d_\Phi\dot{\Phi})}{\sqrt{\Psi}} \tag{92}$$

the condition (90) becomes

$$\mathcal{N}_\Psi'(2+\Psi_{C0})\,\frac{1+c_\Phi\overline{\beta^2}}{S_3}. \tag{93}$$

7.3 The (Ψ,Φ)-Controller for Left-Skew Compressors. For left-skew compressors, for which $S_1<0$, we recover our earlier result (Krstic et al. [5])

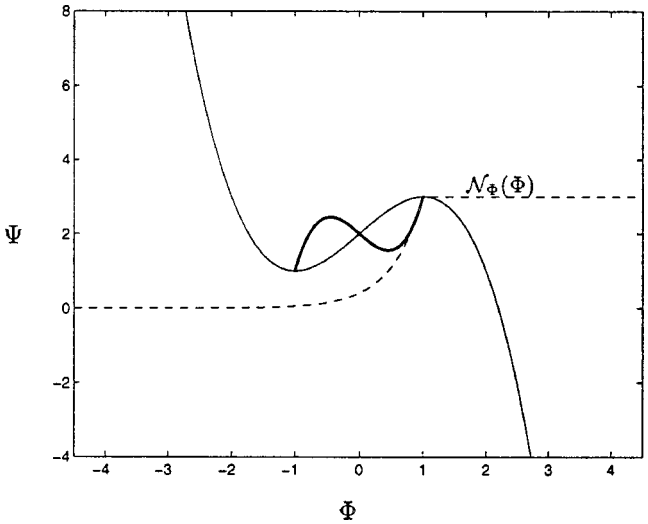

Fig. 11 The function $\mathcal{N}_\Phi(\Phi)$

$$\gamma = \frac{\Gamma + \overline{\beta}^2 (c_\Psi \Psi - c_\Phi \Phi)}{\sqrt{\Psi}} \tag{94}$$

where

$$c_* > 0, \quad c_\Psi > 0, \quad c_* > S_3 c_\Psi . \tag{95}$$

Again, (94) can be replaced by

$$\gamma = \frac{\Gamma + \overline{\beta}^2 c_\Psi (\Psi - \mathcal{N}_\Phi(\Phi))}{\sqrt{\Psi}} \tag{96}$$

where $\mathcal{N}_\Phi(\Phi)$ is sketched in Fig. 11 and satisfies

$$\mathcal{N}'_\Phi(1) > S_3 - \frac{1}{\overline{\beta}^2 c_\Psi}. \tag{97}$$

7.4 A Linear Implementation. Instead of (23), local stability can be achieved with a controller of the form

$$\gamma = \gamma_0 + k_R R - k_\Phi (\Phi - 1) + k_\Psi (\Psi - 2 - \Psi_{C0}) - k_{\dot\Phi} \dot\Phi \tag{98}$$

where γ_0 is a set point/disturbance parameter and the gains k_R, k_Φ, k_Ψ, and $k_{\dot\Phi}$ are required to satisfy

$$k_R - S_1 \left(k_\Phi + \frac{1}{\sqrt{2 + \Psi_{C0}}} \right) + S_2 \left(k_\Psi + \frac{2 + \Phi_{C0}}{2(2 + \Psi_{C0})^{3/2}} \right) > 0 \tag{99}$$

$$k_\Phi + \frac{1}{\sqrt{2 + \Psi_{C0}}} > 0 \tag{100}$$

$$k_{\dot\Phi} + k_\Psi + \frac{2 + \Phi_{C0}}{2(2 + \Psi_{C0})^{3/2}} > 0. \tag{101}$$

For a cubic characteristic, these conditions have already been revealed by Krener [14]. Since these conditions involve not only the shape parameters S_1 and S_2 of the compressor characteristic but also the value of pressure at the peak, $2 + \Psi_{C0}$, we are of the opinion that controller (23), in which Γ is the bifurcation parameter, is preferable to the controller (98).

For right-skew compressors, for which $S_1 > 0$ and $S_2 < 0$, the conditions (99)–(101), in particular, allow controllers of the following types:

$$\gamma = \gamma_0 + k_R R - k_{\dot\Phi} \dot\Phi \tag{102}$$

$$\gamma = \gamma_0 + k_R R + k_\Psi (\Psi - 2 - \Psi_{C0}) \tag{103}$$

$$\gamma = \gamma_0 + k_\Psi (\Psi - 2 - \Psi_{C0}) - k_{\dot\Phi} \dot\Phi. \tag{104}$$

The controller (102) is the familiar UTRC-controller (Eveker et al. [4]). For left-skew compressors, the controller types can also be

$$\gamma = \gamma_0 - k_\Phi (\Phi - 1) + k_\Psi (\Psi - 2 - \Psi_{C0}) \tag{105}$$

$$\gamma = \gamma_0 - k_\Phi (\Phi - 1) - k_{\dot\Phi} \dot\Phi. \tag{106}$$

The PD controller (106) was proposed in Badmus et al. [15].

8 Control Design with Actuator Dynamics

8.1 Stability Conditions. In practical application, the actuator dynamics are the key factor that affects the ability to control compressor instabilities. In this section, we consider the controller with a time lag:[5]

$$\gamma = \frac{1}{\tau s + 1} u, \quad u = \frac{\Gamma + \overline{\beta}^2 (c_\Psi \Psi - c_\Phi \Phi + c_R R - d_\Phi \dot\Phi)}{\sqrt{\Psi}}. \tag{107}$$

With the controller (107), the system (1)–(3) becomes

$$\dot R = \sigma R \mathcal{F}(R, \Phi) \tag{108}$$

$$\dot\Phi = -\Psi + \mathcal{G}(R, \Phi) \tag{109}$$

$$\dot\Psi = \frac{1}{\beta^2} (\Phi + 1 + \Phi_{C0} - \gamma \sqrt{\Psi}) \tag{110}$$

$$\dot\gamma = -\frac{1}{\tau} \gamma + \frac{1}{\tau \sqrt{\Psi}} (\Gamma + \overline{\beta}^2 (c_R R - c_\Phi \Phi + c_\Psi \Psi - d_\Phi \dot\Phi)). \tag{111}$$

Let us consider an equilibrium on the stall characteristic. Define the error coordinates as (36)–(38) and $\tilde\gamma = \gamma - \gamma_0(R_0) = \gamma - (1 + \Phi_{C0} + \Phi_{R+}(R_0))/\sqrt{\Psi_{R+}(R_0)}$. The linearization of the system (108)–(111) is readily shown to be

$$\dot r = -a_1(R_0)(-\Sigma_1(R_0) r + \phi) \tag{112}$$

$$\dot\phi = (\Sigma_2(R_0) + a_2(R_0)\Sigma_1(R_0)) r - a_2(R_0)\phi - \psi \tag{113}$$

$$\dot\psi = \frac{1}{\beta^2} \left(\phi - \sqrt{\Psi_{R+}(R_0)}\, \tilde\gamma - \frac{\beta^2}{\tau_P(R_0)} \psi \right) \tag{114}$$

$$\dot{\tilde\gamma} = \frac{\overline{\beta}^2}{\tau \sqrt{\Psi_{R+}(R_0)}} \left(c_R r + \left(-\frac{1}{\kappa \tau_P(R_0)} + c_\Psi \right) \psi - c_\Phi \phi - d_\Phi \dot\phi \right) - \frac{1}{\tau} \tilde\gamma, \tag{115}$$

where

$$\tau_P(R) \triangleq \frac{2\beta^2 \Psi_{R+}(R)}{1 + \Phi_{C0} + \Phi_{R+}(R)} = \frac{2\beta^2}{2 + \Phi_{C0}} \left[2 + \Psi_{C0} + \left(S_2 - \frac{2 + \Psi_{C0}}{2 + \Phi_{C0}} S_1 \right) R + O(R^2) \right] \tag{116}$$

is referred to as the time constant of the plenum.

With the linearized model (112)–(115), we investigate the stability conditions for this system. The Jacobian of the system (112)–(115) is

$$\begin{bmatrix} a_1 \Sigma_1 & -a_1 & 0 & 0 \\ \Sigma_2 + a_2 \Sigma_1 & -a_2 & -1 & 0 \\ 0 & \frac{1}{\beta^2} & -\frac{1}{\tau_P} & -\frac{\sqrt{\Psi_{R+}(R_0)}}{\beta^2} \\ \xi [c_R - (\Sigma_2 + a_2 \Sigma_1) d_\Phi] & -\xi (c_\Phi - a_2 d_\Phi) & \xi \left(-\frac{1}{\kappa \tau_P} + c_\Psi + d_\Phi \right) & -\frac{1}{\tau} \end{bmatrix}, \tag{117}$$

[5] More realistic actuator models—involving nonlinear magnitude and rate saturation—although possible, would not be analytically tractable.

Table 4 The stability conditions for the system (108)–(111)

$$c_R - S_1\left(c_\Phi + \frac{1}{\overline{\beta}^2}\right) + S_2 c_\Psi > 0$$

$$c_\Phi + \frac{1}{\overline{\beta}^2} > 0$$

$$c_\Psi + d_\Phi + \frac{\tau}{\overline{\beta}^2} > \left(\frac{1}{\tau} + \frac{2+\Phi_{C0}}{2\overline{\beta}^2(2+\Psi_{C0})}\right)^{-1}\left(c_\Phi + \frac{1}{\overline{\beta}^2}\right)$$

where $\xi(R) = \overline{\beta}^2/\tau\sqrt{\Psi_{R+}(R)}$. The characteristic polynomial of the Jacobian (117) is

$$\begin{aligned} p(s) = s^4 &+ \left(a_2 - a_1\Sigma_1 + \frac{1}{\tau} + \frac{1}{\tau_P}\right)s^3 + \left[a_1\Sigma_2 + \frac{\kappa}{\tau}(c_\Psi + d_\Phi)\right. \\ &\left. + \left(\frac{1}{\tau} + \frac{1}{\tau_P}\right)(a_2 - a_1\Sigma_1) + \frac{1}{\beta^2}\right]s^2 + \left[a_1\Sigma_2\left(\frac{1}{\tau} + \frac{1}{\tau_P}\right)\right. \\ &\left. + \frac{\kappa}{\tau}(a_2 - a_1\Sigma_1)c_\Psi - \frac{\kappa}{\tau}a_1\Sigma_1 d_\Phi - \frac{1}{\beta^2}a_1\Sigma_1 + \frac{\kappa}{\tau}c_*\right]s \\ &+ \frac{\kappa}{\tau}a_1[c_R - \Sigma_1 c_* + \Sigma_2 c_\Psi]. \end{aligned} \tag{118}$$

Sufficient conditions for stability of the system near the stall inception point are readily deduced from (118) and are given in Table 4. A center manifold argument similar to that in Section 6.3 proves stability at the bifurcation point.

We point out that in the case of a linear implementation (98), the gains k_R, k_Φ, k_Ψ, and $k_{\dot\Phi}$ are required to satisfy conditions (99) and (101), whereas the condition (100) is modified as

$$\begin{aligned} k_{\dot\Phi} + k_\Psi + \frac{2+\Phi_{C0}}{2(2+\Psi_{C0})^{3/2}} + \frac{\tau}{\sqrt{2+\Psi_{C0}}} \\ > \left(\frac{1}{\tau} + \frac{2+\Phi_{C0}}{2\beta^2(2+\Psi_{C0})}\right)^{-1}\left(k_\Phi + \frac{1}{\sqrt{2+\Psi_{C0}}}\right). \end{aligned} \tag{119}$$

8.2 Actuator/Sensor Trade-Off. The time constant τ appears only in the third condition in Table 4. When $c_\Phi = 0$, this condition becomes

$$c_\Psi + d_\Phi + \frac{\tau^2}{\tau + 2\beta^2\dfrac{2+\Psi_{C0}}{2+\Phi_{C0}}}\frac{1}{\overline{\beta}^2} > 0, \tag{120}$$

i.e., τ does not appear to be harmful, at least near the stall inception point.

However, when β is large, $\overline{\beta}$ has to be selected large (because, if κ is small, the range of stabilized stall equilibria may be infinitesimal). Then we need $c_\Phi > 0$ to maintain a robustness margin (for equilibria further away from the stall inception point) in the second condition in Table 4. When c_Φ is substantial, the effect of τ on the third condition in Table 4 becomes detrimental. In that case, $c_\Psi + d_\Phi$ has to be large enough. We now analyze two possibilities for right-skew compressors ($S_1 > 0, S_2 < 0$) with large β. Our objective is to design controllers with either $d_\Phi = 0$ or $c_R = 0$ in order to relax the sensing requirements.

1 $d_\Phi = 0$. Since $c_\Phi > 0$ and $\tau > 0$, the third condition in Table 4 implies that $c_\Psi > 0$ needs to be sufficiently large, and the first condition implies that $c_R > 0$ needs to be sufficiently large.

2 $c_R = 0$. The first condition in Table 4 implies that $c_\Psi < 0$ needs to be sufficiently large. The third condition implies that $d_\Phi > 0$ needs to be sufficiently large.

The preceding analysis shows that

- If $c_\Phi = 0$ (for example, because β is small), then a larger value of τ can be tolerated without having to increase c_R or d_Φ.
- If $c_\Phi > 0$ (for example, because β is large), then a larger value of τ results in a requirement for larger values of either c_R or d_Φ.

The second point reveals a clear actuator/sensor trade-off: a low-bandwidth valve can be employed only if a good sensor of R or $\dot\Phi$ is available (and vice-versa).

Finally, we point out that, in the presence of τ, the controller from Section 7.3 for left-skew compressors no longer guarantees stability. The first and third conditions in Table 4 yield the condition

$$c_\Psi\left(\frac{1}{\tau} + \frac{2+\Phi_{C0}}{2\beta^2(2+\Psi_{C0})} - \frac{S_2}{S_1}\right) + \frac{\tau(2+\Phi_{C0}) + 2\beta^2(2+\Psi_{C0})}{2\overline{\beta}^2\beta^2(2+\Psi_{C0})} > 0, \tag{121}$$

in which c_* is eliminated. Since S_2/S_1 is always a large positive number for left-skew compressors, c_Ψ can be found to satisfy condition (121) only if τ is sufficiently small.

8.3 Challenge of High-Speed, Many Stage Compressor. As we explained above, for compressors with high β, we need $c_\Phi > 0$. Then the third condition in Table 4 becomes very difficult to satisfy when both τ and $\beta^2(2(2+\Psi_{C0})/(2+\Phi_{C0}))$ are large. In other words, a high-speed, many stage compressor is very hard to control using a low-bandwidth actuator. In fact, it is fair to say that the control problem for this case becomes impossible because, even if we employ high $c_\Psi + d_\Phi$, the actuator saturation will become a problem due to high gains.

9 Bifurcation Diagrams With Control

We now compute bifurcation diagrams for the controllers that we derived in Sections 7 and 8. As a bifurcation parameter, we take Γ. This is based on the observation that the modeling information about the exact shape of the compressor and stall characteristics enters the control law (23) only through Γ which is given by (28). Thus, by treating Γ as the bifurcation parameter, we study an operating scenario where the compressor curves are uncertain and subject to change.

Since in our control design one of the main objectives is to reduce the sensitivity to uncertainties, that is, the sensitivity to Γ, our bifurcation analysis will be primarily concerned with maximizing the interval of post-stall values of Γ for which the stall equilibrium is stable.

We consider a compressor from (Evker et al. [4]) with $\Psi_{C0} = 0.72$, $\sigma = 4$, and a range of values of β. Our numerical tests are performed on the ϵ-MG3 model.

9.1 Left-Skew Case. If they satisfy conditions in Table 4, all of the controllers designed in Sections 7 and 8 achieve a supercritical bifurcation with respect to the parameter Γ. However, we require not only that the bifurcation be supercritical (in which case the stall inception point is guaranteed to be stable), but also that a sufficiently large interval of Γ with stable stall equilibria be achieved. We plot all the bifurcation diagrams with $\Gamma - \Gamma_0$ on the abscissa, where Γ_0 is the value of Γ corresponding to the stall inception point for a given controller. Note that Γ_0 depends on the control gains. The purpose of the shift by Γ_0 is to position the stall inception at zero for all the controllers, to allow an easy comparison of the sensitivity with respect to Γ.

Figure 12 shows a compressor with $\epsilon = 0$ (left-skew), $\beta = 1.42$ (high-speed), $\tau = 0.44$ (a value suggested by Meyers et al. [12],

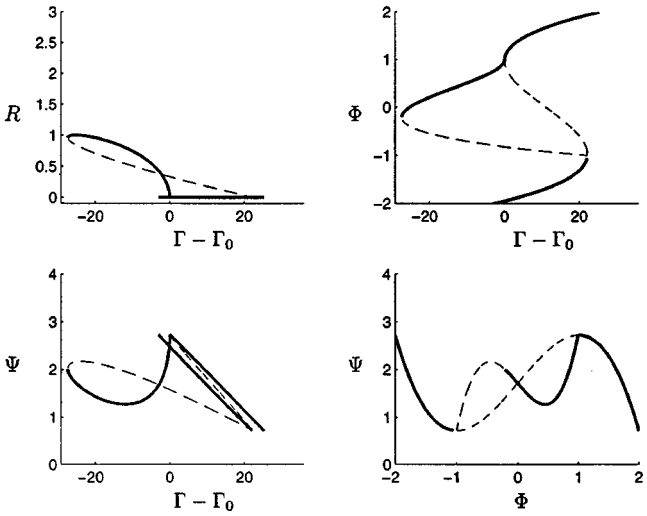

Fig. 12 Bifurcation diagrams for the case $\epsilon=0$, $\beta=1.42$, $\tau=0.44$, with the (Ψ,R)-controller. The control gains are $c_R=18$ and $c_\Psi=6$.

converted to our coordinates), controlled by the (Ψ,R)-controller with gains $c_R=18$, $c_\Psi=6$. The interval of stabilized values of Γ is large.

Our extensive simulations show that both the full-state feedback controller and the two partial-state feedback controllers, (Ψ,R) and $(\Psi,\dot{\Phi})$, can achieve satisfactory behavior even for high β and τ (of course, at the expense of higher gains). The (Ψ,Φ)-controller, however, fails in the presence of τ because the third condition in Table 4 is violated.

9.2 Right-Skew Case. This section shows that the right-skew case is much harder. Even when we satisfy conditions from Table 4 (which guarantee stability of the stall inception point), the interval of stabilized stall equilibria near the peak may be infinitesimally short, and may not be improved by selecting different gains. This illustrates our claim that controllers designed for left-skew models are not applicable to actual compressors which are right-skew. Throughout this section we use $\epsilon=0.9$.

9.2.1 (Ψ,R)*-Controller.* Our extensive simulations show that, even for the ''easy'' case $\beta=0.71$ and $\tau=0$, the interval of stall equilibria that can be stabilized using the (Ψ,R)-controller is infinitesimal. Figure 13 shows the best diagrams achievable with this controller, obtained with gains $c_R=3$, $c_\Psi=1$.

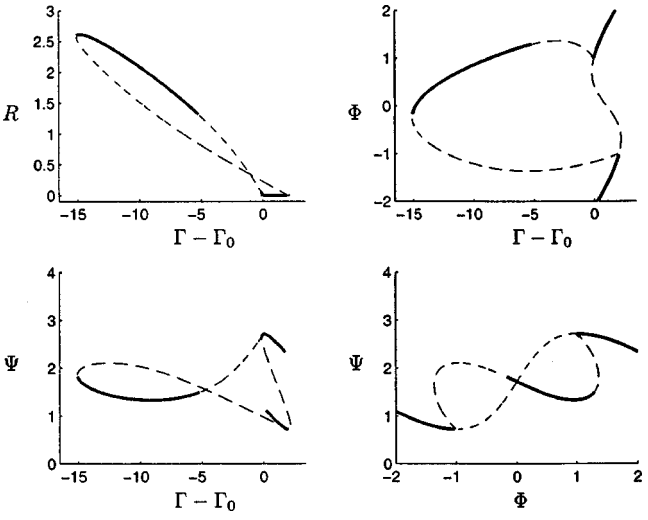

Fig. 13 Bifurcation diagrams for the case $\epsilon=0.9$, $\beta=0.71$, with the (Ψ,R)-controller. The control gains are $c_R=3$ and $c_\Psi=1$.

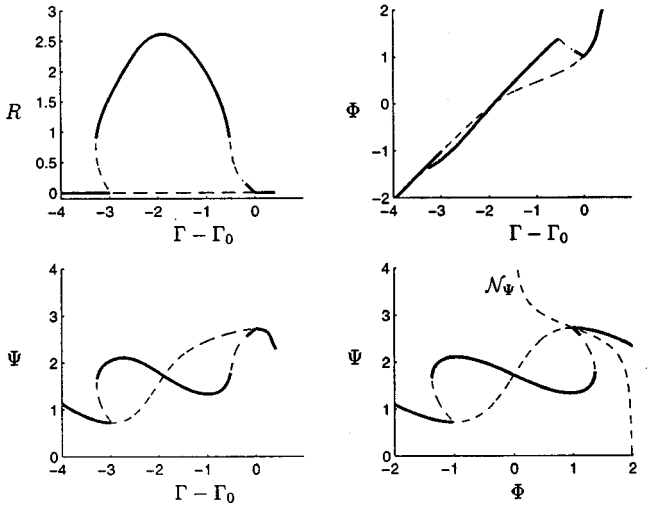

Fig. 14 Bifurcation diagrams for the case $\epsilon=0.9$, $\beta=0.71$, with the nonlinear $(\Psi,\dot{\Phi})$-controller. The controls are gain $d_\Phi=2$ and nonlinear function $\mathcal{N}_\Psi(\Psi)$.

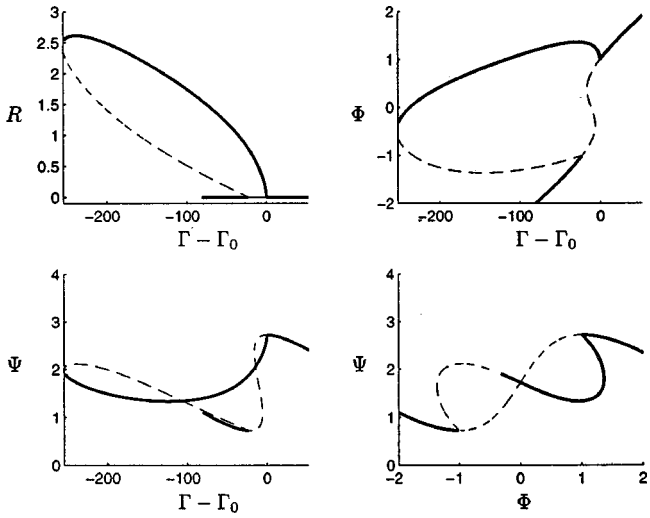

Fig. 15 Bifurcation diagrams for the case $\epsilon=0.9$, $\beta=1.42$, $\tau=0.44$, with the full-state controller. The control gains are $c_R=43$, $c_\Psi=17$, and $c_\Phi=22$.

9.2.2 $(\Psi,\dot{\Phi})$*-Controller.* With this controller it is possible to achieve slightly better results than with the (Ψ,R)-controller. Figure 14 shows diagrams for $\beta=0.71$, $\tau=0$ with gains $c_\Psi=-1$, $d_\Phi=2$, and $\mathcal{N}_\Psi(\Psi)=-2(\Psi-2.72)/\sqrt{1+4(\Psi-2.72)^2}$. When β is increased to $\beta=1.42$, the interval of stable equilibria shrinks.

9.2.3 Full-State Controller. The full-state controller can successfully handle right-skew compressors. Figure 15 shows diagrams for the case $\beta=1.42$, $\tau=0.44$, with gains, $c_R=43$, $c_\Psi=17$, $c_\Phi=22$.

10 Stability on the Stall Branch

It is a general belief in the compressor control community (based on the dramatic results of Eveker et al. [4]) that, since feedback of $\dot{\Phi}$ is beneficial for a left skew compressor, it may be beneficial for a right skew compressor too. We investigate this

conjecture by studying the stability interval under the stall inception point on the stall branch, and show that the conjecture is not true.

We first discuss the impact of the $\dot{\Phi}$-term on the nonlinear controller implementation

$$\gamma = \frac{\Gamma + \overline{\beta}^2 (c_\Psi \Psi - c_\Phi \Phi + c_R R - d_\Phi \dot{\Phi})}{\sqrt{\Psi}}, \tag{122}$$

and then on the linear implementation

$$\gamma = \gamma_0 + k_R R - k_\Phi (\Phi - 1) + k_\Psi (\Psi - 2 - \Psi_{C0}) - k_{\dot{\Phi}} \dot{\Phi}, \tag{123}$$

whose special case is the UTRC controller (Eveker et al. [4]), $k_\Phi = k_\Psi = 0$.

10.1 Nonlinear Implementation. To make things easy, we set $\tau = 0$ and consider the system (39)–(41). By Routh-Hurwitz and using Lemma 6.1, the necessary and sufficient conditions for stability are (73)–(76), which we respectively denote as

$$h_1(R_0) > 0 \tag{124}$$

$$h_2(R_0) > 0 \tag{125}$$

$$h_3(R_0) > 0 \tag{126}$$

$$h_4(R_0) > 0. \tag{127}$$

They represent stability conditions on the stall branch, away from the stall inception point. We expand the functions h_i about 0 and get

$$h_i(R_0) = h_i(0) + h_i'(0) R_0 + O(R_0^2), \quad i = 1, \ldots, 4. \tag{128}$$

The quantities $h_i(0)$ and $h_i'(0)$ are given in Tables 5 and 6, respectively.

For small $R_0 > 0$ (near the stall inception point), a necessary condition for stability is $h_i(0) + h_i'(0) R_0 > 0$. Let us concentrate on

$$h_2(0) + h_2'(0) R_0 = \kappa \left(c_\Phi + \frac{1}{\overline{\beta}^2} \right) + \left[\kappa S_1 S_2 \left(1 + \frac{2\sigma}{3} \right) c_\Psi - \frac{2\sigma}{3} S_2^2 \right] R_0 + \frac{2\sigma}{3} \kappa S_1 S_2 d_\Phi R_0. \tag{129}$$

Since R_0 is independent of d_Φ, the sign of $h_i(0) + h_i'(0) R_0$ for large d_Φ is determined by the sign of $S_1 S_2 = -\frac{1}{2} \Psi_C'''(1)$. This means that, for large d_Φ,

$$h_i(0) + h_i'(0) R_0 \begin{cases} > 0, & \text{left-skew case} \\ < 0, & \text{right-skew case} \end{cases}$$

Thus, high gain on $\dot{\Phi}$ makes a right-skew compressor unstable. Similar but more complicated argument applies to $h_4(R_0)$.

Table 5 $h_i(0)$ for nonlinear implementation

$h_1(0)$	$\kappa (d_\Phi + c_\Psi)$
$h_2(0)$	$\kappa \left(c_\Phi + \frac{1}{\overline{\beta}^2} \right)$
$h_3(0)$	0
$h_4(0)$	$\kappa^2 (d_\Phi + c_\Psi) \left(c_\Phi + \frac{1}{\overline{\beta}^2} \right)$

Table 6 $h_i'(0)$ for nonlinear implementation

$h_1'(0)$	$\left(1 + \frac{2\sigma}{3} \right) S_1 S_2$
$h_2'(0)$	$\kappa S_1 S_2 \left[\left(1 + \frac{2\sigma}{3} \right) c_\Psi + \frac{2\sigma}{3} d_\Phi \right] - \frac{2\sigma}{3} S_2^2$
$h_3'(0)$	$-\frac{2\sigma}{3} \kappa S_2 (c_R - S_1 c_* + S_2 c_\Psi)$
$h_4'(0)$	$\kappa S_2 \left\{ \kappa S_1 c_\Psi (d_\Phi + c_\Psi) + S_1 c_* + \frac{2\sigma}{3} \left[\kappa S_1 (d_\Phi + c_\Psi)^2 + c_R - S_2 d_\Phi \right] \right\}$

10.2 Linear Implementation. Tables 7 and 8 are equivalent to Tables 5 and 6, respectively. We use the notation

$$k_{\Phi *} = k_\Phi + \frac{1}{\sqrt{2 + \Psi_{C0}}} \tag{130}$$

$$k_{\Psi *} = k_\Psi + \frac{2 + \Phi_{C0}}{2 (2 + \Psi_{C0})^{3/2}}. \tag{131}$$

A discussion similar to that in Section 10.1 shows that the increase of $k_{\dot{\Phi}}$ results in instability for the right-skew case. Let us now set $k_\Phi = k_\Psi = 0$ and concentrate on the UTRC controller. Since $h_2(0)$ and R_0 are independent of $k_{\dot{\Phi}}$, for stability we require that $h_2'(0) > 0$. It is obvious that, for large $k_{\dot{\Phi}}$, the sign of $h_2'(0)$ is determined by the sign of $S_1 S_2 = -\frac{1}{2} \Psi_C'''(1)$. Thus, the

Table 7 $h_i(0)$ for linear implementation

$h_1(0)$	$\frac{1}{\overline{\beta}^2} \sqrt{2 + \Psi_{C0}} (k_{\dot{\Phi}} + k_{\Psi *})$
$h_2(0)$	$\frac{1}{\overline{\beta}^2} \sqrt{2 + \Psi_{C0}} k_{\Phi *}$
$h_3(0)$	0
$h_4(0)$	$\frac{1}{\overline{\beta}^4} (2 + \Psi_{C0}) (k_{\dot{\Phi}} + k_{\Psi *}) k_{\Phi *}$

Table 8 h_i' for linear implementation

$h_1'(0)$	$\left(1 + \frac{2\sigma}{3} \right) S_1 S_2$
$h_2'(0)$	$\frac{1}{\overline{\beta}^2} S_1 S_2 \sqrt{2 + \Psi_{C0}} \left[\left(1 + \frac{2\sigma}{3} \right) k_{\Psi *} + \frac{2\sigma}{3} k_{\dot{\Phi}} \right] - \frac{2\sigma}{3} S_2^2$
$h_3'(0)$	$-\frac{2\sigma}{3\overline{\beta}^2} S_2 \sqrt{2 + \Psi_{C0}} (k_R - S_1 k_{\Phi *} + S_2 k_{\Psi *})$
$h_4'(0)$	$\frac{1}{\overline{\beta}^2} S_2 \sqrt{2 + \Psi_{C0}} \left\{ \frac{1}{\overline{\beta}^2} S_1 \sqrt{2 + \Psi_{C0}} k_{\Psi *} (k_{\dot{\Phi}} + k_{\Psi *}) + k_{\Phi *} + \frac{2\sigma}{3} \left[\frac{1}{\overline{\beta}^2} S_1 \sqrt{2 + \Psi_{C0}} (k_{\dot{\Phi}} + k_{\Psi *})^2 + k_R - S_2 k_{\dot{\Phi}} \right] \right\}$

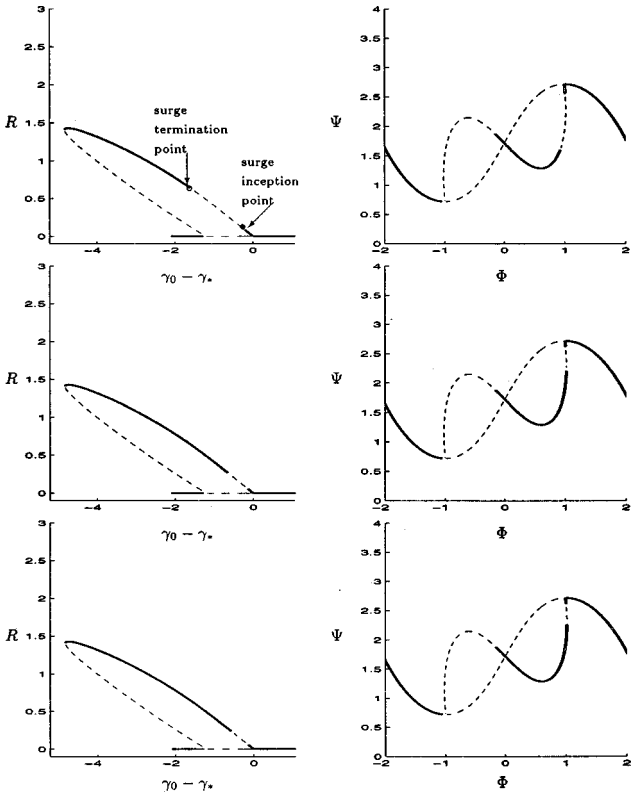

Fig. 16 Closed-loop bifurcation diagrams for $\epsilon = 0.6$ with UTRC controller. The control gains are $k_R = 3$ and $k_{\dot{\Phi}} = 1,10,100$.

increase of $k_{\dot{\Phi}}$ results in stability for the left-skew case and in instability for the right-skew case. Similar argument can be performed for $h_4(R_0)$.

Figure 16 shows results for the slightly right-skew case $\epsilon = 0.6$ where a dramatic change occurs. With $k_{\dot{\Phi}} = 1$, stability is lost very close to the stall inception point, at a point that we refer to as the surge inception point. Stability is recovered at the surge termination point, resulting in a diagram similar to the Liaw-Abed controller. As one increases $k_{\dot{\Phi}}$ to 10 and 100, both the surge inception point and the surge termination point move toward the stall inception point! This is an effect opposite to the effect of the $\dot{\Phi}$-term in the left-skew case (reported by Evker et al. [4]) where the increase in $k_{\dot{\Phi}}$ results in the surge inception point moving away from the stall inception point.

11 Conclusions

The model parametrization that we have derived captures the right-skew property of the Sepulchre-Kokotović model while retaining the relative simplicity of the Moore-Greitzer [1] model. This model can now be easily used in simulations as a replacement of the cubic MG3.

The controllers that we developed offer several solutions to the problem of stabilizing rotating stall and surge in low-order models of deep-hysteresis compressors. By studying different sensing architectures and the effect of the actuator time constant, we revealed an important tradeoff between the ''cost'' of sensing and actuation. Our results show that, if a less expensive (lower-bandwidth) bleed valve is employed, the controller gains have to be higher, which can be implemented only with sensors of better accuracy. Finally, we disproved the conjecture that $\dot{\Phi}$ feedback may be beneficial beyond the class of shallow-hysteresis compressors.

Our main observation is that the task of controlling high-speed many-stage compressors using a low-bandwidth valve is extremely challenging. Furthermore, our simulation study showed that the difficulties for control rapidly increase with the increase of right-skewness. This brings up a natural question (posed by an insightful reviewer): are difficulties due to a poor control law or a questionable actuation scheme. Since the control law is state feedback whose parameter space was searched exhaustively in our case study, it is obvious that the difficulties are due to the choice of actuation via bleed valve. While we acknowledge that bleed valve control has shown success for left-skew low-speed compressors (Eveker et al. [4]), we point out the following. Rather than searching for bleed valves of unreasonably high bandwidth, future effort in compressor control should perhaps focus on exploring opportunities for using close coupled valves (Simon et al. [16]) and air injection (Behnken et al. [7]).

Acknowledgment

We would like to thank the following people for their impact on this paper: A. Banaszuk, K. Eveker, D. Fontaine, D. Gysling, P. Kokotovic, A. Krener, R. Murray, M. Myers, C. Nett, J. Paduano, and R. Sepulchre.

References

[1] Moore, F. K., and Greitzer, E. M., 1986, ''A Theory of Post-Stall Transients in Axial Compression Systems—Part I: Development of Equations,'' ASME J. Eng. Gas Turbines Power, **108**, pp. 68–76.
[2] Liaw, D.-C., and Abed, E. H., 1996, ''Active Control of Compressor Stall Inception: A Bifurcation-Theoretic Approach,'' Automatica, **32**, pp. 109–115, also in *Proceedings of the IFAC Nonlinear Control Systems Design Symposium*.
[3] Badmus, O. O., Chowdhury, S., Eveker, K. M., Nett, C. N., and Rivera, C. J., 1993, ''A Simplified Approach for Control of Rotating Stall, Parts I and II,'' *Proceedings of the 29th Joint Propulsion Conference*, AIAA papers 93-2229 & 93-2234.
[4] Eveker, K. M., Gysling, D. L., Nett, C. N., and Sharma, O. P., 1995, ''Integrated Control of Rotating Stall and Surge in Aeroengines,'' *1995 SPIE Conference on Sensing, Actuation, and Control in Aeropropulsion*.
[5] Krstić, M., Fontaine, D., Kokotović, P. V., and Paduano, J. D., 1998, ''Useful Nonlinearities and Global Bifurcation Control of Jet Engine Surge and Stall,'' IEEE Trans Automatic Control, **43**, pp. 1739–1745.
[6] Mansoux, C. A., Setiawan, J. D., Gysling, D. L., and Paduano, J. D., 1994, ''Distributed Nonlinear Modeling and Stability Analysis of Axial Compressor Stall and Surge,'' *1994 American Control Conference*.
[7] Behnken, R. L., D'Andrea, R., and Murray, R. M., 1995, ''Control of Rotating Stall in a Low-speed Axial Flow Compressor Using Pulsed Air Injection: Modeling, Simulations, and Experimental Validation,'' *Proceedings of the 1995 IEEE Conference on Decision and Control*, pp. 3056–3061.
[8] Jankovic, M., 1995, ''Stability Analysis and Control of Compressors with Noncubic Characteristic,'' PRET Working Paper B95-5-24.
[9] Sepulchre, R., and Kokotović, P. V., 1998, ''Shapes Signifiers for Control of Surge and Stall in Jet Engines,'' IEEE Transactions on Automatic Control, **43**, pp. 1643–1648.
[10] McCaughan, F. E., 1990, ''Bifurcation Analysis of Axial Flow Compressor Stability,'' SIAM (Soc. Ind. Appl. Math.) J. Appl. Math., **20**, pp. 1232–1253.
[11] Wang, H.-H., Krstić, M., and Larsen, M., 1997, ''Control of Deep-Hysteresis Aeroengine Compressors—Part I: A Moore-Greitzer Type Model,'' *Proc. 1997 American Control Conference*, pp. 1003–1007.
[12] Meyers, M. R., Gysling, D. L., and Eveker, K. M., 1995, ''Benchmark for Control Design: Moore-Greitzer Model,'' PRET Working Paper, UTRC95-9–18.
[13] Khalil, H. K., 1996, *Nonlinear Systems*, Second Edition, Prentice Hall, Englewood Cliffs, NJ.
[14] Krener, A. J., 1995, ''The Feedbacks Which Soften the Primary Bifurcation of MG3,'' PRET Working Paper B95-9-11.
[15] Badmus, O. O., Nett, C. N., and Schork, F. J., 1991, ''An Integrated, Full-Range Surge Control/Rotating Stall Avoidance Compressor Control System,'' *Proceedings of the 1991 American Control Conference*, pp. 3173–3180.
[16] Simon, J. S., Valavani, L., Epstein, A. H., and Greitzer, E. M., 1993, ''Evaluation of approaches to active compressor surge stabilization,'' ASME J. Turbomachinery, **115**, pp. 57–67.